Pergamon

Int. J. Heat Mass Transfer. Vol. 37, No. 10, pp. 1495–1508, 1994

0017-9310/94 $7.00+0.00

0017-9310-(93)E0093-V

An improved low-Reynolds-number κ–ε turbulence model for recirculating flows

H. H. CHO and R. J. GOLDSTEIN

Heat Transfer Laboratory, Department of Mechanical Engineering, University of Minnesota, Minneapolis, MN 55455, U.S.A.

(*Received* 20 *May* 1993 *and in final form* 12 *November* 1993)

Abstract—A revised form of the low-Reynolds-number κ–ε turbulence model is presented that aptly describes recirculating (separated and reattached) flows. The revised model is well suited for low to moderate Reynolds numbers. It is applied to two-dimensional channel flows, flow over a backward facing step, and flow over a forward facing step to calculate flow fields and surface heat or mass transfer rates. Results from the present model are in better agreement with experimental data than other low-Reynolds-number models. Asymmetric flow through an array of rectangular cylinders, as well as in a two-dimensional symmetric sudden expansion duct, is found numerically and supported by experimental results.

INTRODUCTION

THE GOAL of the present study is to model turbulent flow in separated regions, and to show the instability of flow in a symmetric geometry using a numerical method. The flow field in many engineering systems contains separation, reattachment, and recirculation regions. The heat transfer augmentation that occurs with separation and reattachment is common to many engineering devices and the prediction of separated flow and the subsequent heat transfer is of practical importance. Present turbulence models do not adequately predict separated flows and heat transfer. The heat transfer rates near the reattachment point are strongly affected by separation, as they increase rapidly and then decay more slowly than those of ordinary boundary layer flows.

There are two dominant factors in the near wall region. One is the local low turbulent Reynolds number effect; the laminar viscosity becomes more important as one approaches the wall. The other factor close to a wall is the damping of the turbulent fluctuations in the direction normal to the wall.

Generally, there are two numerical methods for considering near wall regions; wall function methods and low Reynolds number turbulence models. The high Reynolds number κ–ε model is not generally applicable to near-wall flows because of the low turbulent Reynolds number effects and the wall damping effects. To alleviate these problems, the high Reynolds number turbulence model uses a wall function which connects the surface boundary to a point in the fully turbulent region. The wall function is restricted to situations where a universal law (i.e. law of the wall) exists. The wall functions and high Reynolds number turbulence model cannot properly evaluate separation flows. The low-Reynolds-number κ–ε model adopts the empirical functions of f_μ, f_1, and f_2 (see equations (2) and (4)) in the near wall region with fine grids. The functions are derived to give results which are similar to the wall function in the high Reynolds number turbulence model. Generally, most of the flow field is not strongly dependent on the near wall turbulence model. However, the heat transfer rate on the wall is very sensitive to the model because the main temperature difference (up to 50%) is located in the thin near-wall region and the heat must transfer through the viscous sublayer by molecular diffusion. It is difficult to predict adequately the heat transfer rates along the wall even with a satisfactory prediction of the flow field, hence the numerical model in this near wall region is important for heat transfer. Unfortunately, the low-Reynolds-number turbulence models seem to predict heat transfer rates that are too high in the reattachment region after separation, as shown by Chieng and Launder [1]. Inside the recirculation zone, the velocities are low, yet the level of turbulent kinetic energy is relatively high. This results from diffusion/transport from the bordering shear layer, where high turbulence is generated. However, the dissipation of turbulent kinetic energy is small in this zone because of large eddy motions rather than small eddy motions. Thus, the near wall zone in the recirculation bubble (close to reattachment) has high turbulence levels and therefore high heat transfer rates.

The local turbulent Reynolds number decreases close to the wall. The molecular viscosity becomes important in the balance of turbulent kinetic energy and dissipation. The low-Reynolds-number turbulence model, to calculate flow in the near wall region, was originally proposed by Jones and Launder [2, 3]. The wall proximity is accounted for by modifying the original high Reynolds number κ–ε model.

NOMENCLATURE

b channel width
C_f skin friction coefficient
$C_\mu, C_{\varepsilon 1}, C_{\varepsilon 2}$ constants in turbulence model (equation (2) and Table 1)
D, E additional terms in turbulence model, $D = \varepsilon - \varepsilon_0$
D_h hydraulic diameter in duct
f_1 coefficient of the generation term of ε (equation (2) and Table 1)
f_2 correction function of the destruction term of ε (equation (2) and Table 1)
f_μ damping function to account for laminar viscosity to μ_t (equation (4) and Table 1)
G production of κ (equation (5))
H step height in backward facing step flow and sudden expansion duct
h_1, h_2 channel heights in converging step flow
K acceleration parameter, $\nu(\mathrm{d}U_m/\mathrm{d}x)(1/U_m^2)$
L_w size of wake behind a cylinder (in streamwise direction)
Nu Nusselt number
P pitch of an array of cylinders
$Re(L)$ Reynolds number based on the characteristic length L, UL/ν
R_t turbulent Reynolds number, $\kappa^2/\nu\,\varepsilon$
R_y turbulent Reynolds number, $\sqrt{\kappa}y/\nu$
S slit width in an array of rectangular cylinders
Sh Sherwood number
St Stanton number
T time mean temperature
T_∞ free stream temperature
U, V time mean velocity in Cartesian coordinates
U_c centerline velocity
U_m upstream channel mean velocity
U_{ref} free stream velocity
u_i' fluctuating velocity
u_τ friction velocity, $\sqrt{\tau_w/\rho}$
u^+ dimensionless velocity, u/u_τ
W, W_0 channel heights in sudden expansion ducts
x, y Cartesian coordinates
x_n coordinate in normal direction on the wall
x_P position along the periphery of the cylinder
x_R reattachment length (separation zone size)
x^* dimensionless length scale, $(x-x_R)/x_R$
y^+ dimensionless distance, $u_\tau y/\nu$.

Greek symbols
δ boundary layer thickness
$\varepsilon, \varepsilon_0$ dissipation rate of turbulent kinetic energy ($\varepsilon_0 = \varepsilon - D$ and equation (6))
κ turbulent kinetic energy, $\frac{1}{2}\overline{u_i'u_i'}$
κ^+ dimensionless turbulent kinetic energy, κ/u_τ^2
μ dynamic viscosity
μ_t turbulent viscosity
ν kinematic viscosity
ρ density
$\sigma_\kappa, \sigma_\varepsilon$ turbulent Prandtl numbers for diffusion of κ and ε
τ_w wall shear stress.

Subscripts
i, j, k tensor notation
t turbulence value
v value at outer edge of viscous sublayer
w wall value.

Later, several versions of the model were made and improved for various purposes. There is still inadequate prediction of certain flows, especially in recirculation regions. The present model is similar to that of Jones and Launder's model [2, 3], but the detailed forms are quite different. The model is tested on fully developed two-dimensional turbulent channel flows and applied to separated flows over steps. A better prediction is obtained by the present model for the cases considered.

TURBULENCE MODELING

The governing equations for the two-dimensional κ–ε model can be written in the following form:

$$\rho U_j \frac{\partial \kappa}{\partial x_j} = \frac{\partial}{\partial x_j}\left(\left(\mu + \frac{\mu_t}{\sigma_\kappa}\right)\frac{\partial \kappa}{\partial x_j}\right) + G - \rho\varepsilon \quad (1)$$

$$\rho U_j \frac{\partial \varepsilon}{\partial x_j} = \frac{\partial}{\partial x_j}\left(\left(\mu + \frac{\mu_t}{\sigma_\varepsilon}\right)\frac{\partial \varepsilon}{\partial x_j}\right) + (C_{\varepsilon 1} f_1 G - C_{\varepsilon 2} f_2 \rho\varepsilon)\frac{\varepsilon}{\kappa} + E \quad (2)$$

where

$$\varepsilon = \varepsilon_0 + D \quad (3)$$

$$\mu_t = c_\mu f_\mu \rho \frac{\kappa^2}{\varepsilon} \quad (4)$$

$$G = \mu_t\left(\frac{\partial U_i}{\partial x_j} + \frac{\partial U_j}{\partial x_i}\right)\frac{\partial U_i}{\partial x_j}$$

$$= \mu_t\left(2\left(\frac{\partial U}{\partial x}\right)^2 + 2\left(\frac{\partial V}{\partial y}\right)^2 + \left(\frac{\partial V}{\partial x} + \frac{\partial U}{\partial y}\right)^2\right). \quad (5)$$

Here κ is the turbulent kinetic energy and ε is the isotropic dissipation rate of the turbulent kinetic energy.

Table 1 summarizes the constants and functions, including additional terms D and E, for several low-Reynolds-number κ–ε models.

κ equation

Most low-Reynolds-number κ–ε models have an extra term (D in Table 1) which is chosen to give the turbulent dissipation rate near the wall boundary. Those models set $\varepsilon_0 = 0$ ($\varepsilon_0 = \varepsilon - D$) on the wall boundary, although ε is not really zero. The present model uses $D = 0$ as in the original high Reynolds number turbulence model. The reason will be discussed later.

ε equation

The modeling of the ε equation comes from an exact form of the Navier–Stokes equation where the unknown turbulence correlations are approximated by the known terms. The isotropic dissipation rate ε is defined as

$$\varepsilon = \nu \overline{\frac{\partial u_i'}{\partial x_j} \frac{\partial u_i'}{\partial x_j}} \tag{6}$$

in the case of homogeneous turbulence. The low-Reynolds-number turbulence models usually solve for the modified dissipation rate ε_0 ($= \varepsilon - D$), which is assumed zero at the wall boundary, since it is computationally advantageous as discussed by Jones and Launder [2]. The difference is presented by the D term in the κ equation. The solution of the ε_0 equation in those models is not the real dissipation rate and cannot be compared with the experimental data, even if ε_0 might be close to ε except near the wall boundary. The ε_0 values increase very quickly from zero near the wall to match ε values. Many grid points are needed near the wall boundary to follow this rapid variation. It will not be possible when the viscous sublayer is thin resulting from high velocity, because the prediction requires several grid points in the viscous sublayer. Reynolds [4] and Lam and Bremhorst [5] used a wall boundary condition

$$\varepsilon|_w = \nu \frac{\partial^2 \kappa}{\partial y^2}$$

instead of $\varepsilon_0 = 0$ and did not include additional terms in the κ and ε equation. When using ε, the gradient of the dissipation rate can be modeled to zero because Jones and Launder [2] showed that

$$\varepsilon = 2\nu \left(\frac{\partial \kappa^{1/2}}{\partial y} \right)^2$$

near the wall and the turbulent kinetic energy was given by

$$\kappa = \kappa_v \left(\frac{y}{y_v} \right)^2$$

empirically in the viscous sublayer. So,

$$\left. \frac{\partial \varepsilon}{\partial y} \right|_w = 0$$

can be achieved close to the wall. This boundary condition is selected for computational advantages since it models a physically realistic situation. This boundary condition was also used for an algebraic stress model by Hanjalic and Launder [6].

In a separated flow, reattachment and recirculation, the numerical model usually predicts a turbulent viscosity near the wall that is too high and a viscous sublayer that is thin. Hence, a high heat transfer is predicted. Three additional terms were adopted to increase the dissipation rate near the wall (E in Table 1). The first two terms in S_ε (E term in Table 1) are related to regions near the wall (within the buffer layer) and diminish in the fully turbulent region. The additional empirical terms are added to account for the nonequilibrium dissipation processes. These terms help by adjusting the turbulent dissipation rate from the fully turbulent region to the viscous sublayer. The last term is adopted from Yap [7] which is a correction term of non-homogeneous turbulent flow and gives a better prediction of heat transfer rate near the reattachment point. The coefficients of these terms are usually chosen by computational optimization. All these terms should diminish in fully turbulent regions to match the basic high-Reynolds-number κ–ε model.

f_μ

The low-Reynolds-number model adopts a damping function f_μ to account for the laminar viscosity μ to the turbulent viscosity μ_t at the low turbulent Reynolds number near the wall (viscous sublayer and buffer zone).

Patel *et al.* [8] reviewed several low-Reynolds-number κ–ε models and showed that the Lam and Bremhorst [5] model (abbreviated to LB hereafter) gave the best approximation with experimental data. Recently, Xu and Yang [9] also reviewed the low-Reynolds-number κ–ε models for turbulent wall jets, and argued that the NH model [10] was in the best agreement. However, these two models contain R_y or y^+ in the correction equation which can be chosen arbitrarily from two different length dimensions in a complex geometry (e.g. a right angle corner). The turbulent structure in the recirculation zone or near the reattachment zone is different from that in normal boundary layer flow (i.e. different log-law slope and viscous sublayer thickness). The coefficient of f_μ in the NH model, which is equivalent to the Van Driest damping, would be changed in the recirculation zone or near the reattachment point. The f_μ would be best applied using a function of R_t, R_y, and y^+. However,

Table 1. Constants and functions for several κ–ε models

Model	Abr.	ε_w-BC	C_μ	$C_{\varepsilon 1}$	$C_{\varepsilon 2}$	σ_κ	σ_ε	f_μ	f_1	f_2	D	E
High *Re*	HR	wall fnt	0.09	1.44	1.92	1.0	1.3	1.0	1.0	1.0	0	0
Launder–Sharma [23]	LS	0	0.09	1.44	1.92	1.0	1.3	$\exp[-3.4/(1+R_t/50)^2]$	1.0	$1-0.3\exp(-R_t^2)$	$2\nu\left(\frac{\partial\sqrt{\kappa}}{\partial y}\right)^2$	$\frac{2\mu\mu_t}{\rho}\left(\frac{\partial^2 U}{\partial y^2}\right)^2$
Lam–Bremhorst [5]	LB	$\nu\frac{\partial^2\kappa}{\partial y^2}$	0.09	1.44	1.92	1.0	1.3	$[1-\exp(-0.165R_y)]^2 \times(1+20.5/R_t)$	$1+(0.05/f_\mu)^3$	$1-\exp(-R_t^2)$	0	0
Nagano–Hishida [10]	NH	0	0.09	1.45	1.9	1.0	1.3	$[1-\exp(-y^+/26.5)]^2$	1.0	$1-0.3\exp(-R_t^2)$	$2\nu\left(\frac{\partial\sqrt{\kappa}}{\partial y}\right)^2$	$(1-f_\mu)\frac{\mu\mu_t}{\rho}\left(\frac{\partial^2 U}{\partial y^2}\right)^2$
Present	Pr	$\frac{\partial\varepsilon}{\partial x_n}=0$	0.09	1.44	1.92	1.0	1.3	$1-0.95\exp(-5\times10^{-5}R_t)$	1.0	$1-0.222\exp(-R_t^2/36)$	0	S_ε

$$S_\varepsilon = 1.44(1-f_\mu)\left[\frac{2\mu\mu_t}{\rho}\left(\frac{\partial^2 U_i}{\partial x_j\partial x_k}\right)^2+2\mu\left(\frac{\partial\sqrt{\kappa}}{\partial x_i}\right)^2\frac{\varepsilon}{\kappa}\right]+\max\left[0.83\frac{\varepsilon^2}{\kappa}\left(\frac{l}{C_l x_n}-1\right)\left(\frac{l}{C_l x_n}\right)^2, 0.0\right]$$

where

$l=\frac{\kappa^{1.5}}{\varepsilon}$, $C_l=2.44$, and x_n = normal distance from the wall.

the present f_μ is modeled by using the turbulent Reynolds number, R_t, from the channel and step flow experimental data in the near wall region because R_t does not have a physical length dimension.

f_1 and f_2

The coefficients included in the differential equations could depend on the local turbulence Reynolds numbers. The coefficient, f_1, of the generation term of ε, is set at 1 as in the high Reynolds number model, and the corresponding generation of ε in low Reynolds number flow is considered in additional empirical terms of ε equation (E term). The f_2 is a function which corrects the destruction term of ε in low turbulent Reynolds number flow. The present model adopts the function of Chien's model [11] initiated by Hanjalic and Launder [6]. This term goes quickly to a high turbulence form because f_2 rapidly approaches 1 with increasing R_t.

SOLUTION OF THE EQUATIONS

The elliptic partial difference equations have been solved for two dimensional steady flow conditions using the SIMPLER algorithm of Patankar [12]. This program uses staggered and nonuniform grids which give a fine mesh in the near wall region. Inlet conditions are selected from available experimental data in a given geometry, or they are obtained from the well-known flat plate flow data of Klebanoff [13] or the two-dimensional channel flow data of Laufer [14]. The first several grid points are located within the viscous sublayer in all cases. The boundary conditions for turbulent kinetic energy κ and the gradient of dissipation rate ε are set to zero at the wall; the rationale for this was given in the previous section.

NUMERICAL CALCULATION FOR SAMPLE PROBLEMS

Two-dimensional channel flow

Two-dimensional channel flows are considered as a test case. The coefficients of the present model are optimized from the experimental data of the channel flow studied by Laufer [14] and Eckelmann [15]. The numerical results are compared with those of the other models in Table 1. The skin friction coefficients (Table 2) from the other models predict values higher than the experimental data because velocity distributions overshoot. Logarithmic velocity profiles from the other models are underpredicted (Fig. 1(a)). These features also are shown at a higher Reynolds number, 24 000, with Laufer's data [14]. The present model also more accurately predicts the dimensionless turbulent kinetic energy κ^+ (Fig. 1(b)).

Downstream of a backward facing step flow

A two-dimensional backward facing step flow is a simple recirculation flow in which separation occurs at a fixed point, the edge of the step. The heat transfer rate in the recirculation region near the reattachment point is much higher than that in normal boundary layer flow. This results from a high turbulence level (turbulent diffusion coefficient) due to the large length scale motion of the shear flow which generates high turbulent kinetic energy and reduces the dissipation rate.

Launder [16] showed the numerical results from several turbulence models for the downstream region of an abrupt pipe expansion. He shows how much the Nusselt numbers scatter from experimental data in separation and reattachment flow. Gooray *et al.* [17] tried to solve this problem using a two-pass procedure with a standard high Reynolds number κ–ε model in recirculation zone and a low Reynolds number κ–ε model downstream of the reattachment point. They got a better solution than using only one model; however, it could be too complicated in general cases and requires much computational time. Amano [18] used a near-wall three-layer model which showed good agreement with experimental data. Recently, Ciofalo and Collins [19] used an improved wall function treatment and got a good heat transfer rate prediction in single step flow. The distance to the reattachment point, however, was significantly shorter than that found experimentally. Prud'homme and Elghobashi [20] used a full Reynolds stress model and Launder [16] showed that the algebraic stress model was better than the κ–ε model. Again, these models would require much more computational time because they have more differential equations to solve.

The reattachment length (defined from the separation point to the reattachment point) is the most representative parameter in a backward-facing step flow because all flow velocities and temperature fields relate to this value. The reattachment lengths are shown in Table 3 for the numerical predictions and the experimental result (Vogel and Eaton [21]). The other models predict short reattachment lengths.

Table 2. Skin friction coefficients for the two-dimensional channel flow: $(C_f/2) = (\tau_w/\rho U_c^2)$

$Re(H)$	Experiment	LS	NH	LB	Pr
5600	2.57×10^{-3}†	3.29×10^{-3}	3.31×10^{-3}	3.50×10^{-3}	2.67×10^{-3}
8200	2.57×10^{-3}†	3.23×10^{-3}	3.14×10^{-3}	3.35×10^{-3}	2.59×10^{-3}
24 600	1.90×10^{-3}‡	2.58×10^{-3}	2.45×10^{-3}	2.65×10^{-3}	2.18×10^{-3}

† Eckelmann [15].
‡ Laufer [14].

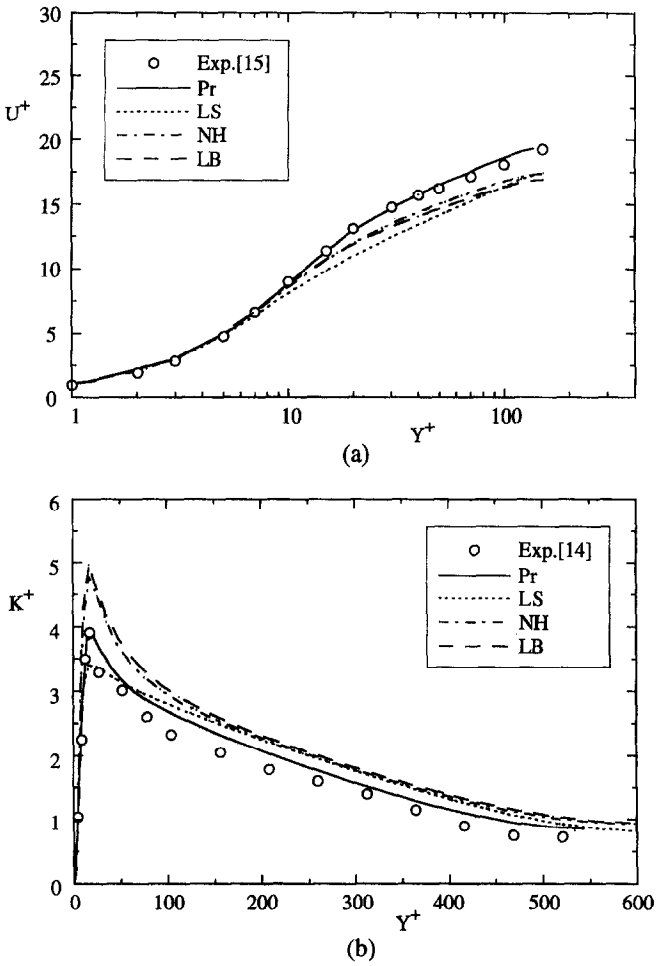

FIG. 1. Comparison of results for two-dimensional channel flows with different models. (a) Logarithmic velocity profiles at $Re(b) = 5600$. (b) Dimensionless turbulent κ–ε profiles at $Re(b) = 24\,000$.

When the streamline curvature effect, proposed by Leschziner and Rodi [22], is considered in the present model, the reattachment length is slightly different and changes in the wrong direction.

The Stanton number profiles on the bottom test plate are shown in Fig. 2 for the different models. The NH and LB models have somewhat unusual predictions, especially near the reattachment point (determined by zero velocity in the mainflow direction at the closest grid point to the wall). This may result from their f_μ functions including y^+ or R_y. The LS model has a high peak value near the reattachment point. This peak for the LS model [23] (improved version of the JL model [2, 3]) was also indicated by Chieng and Launder [1] for sudden expansion pipe flow. All maximum Stanton numbers (including those from experimental data), except in the NH model, occur slightly upstream (about $0.1 \sim 0.2H$) of the reattachment point. However, pressure coefficients on the wall for the models are in good agreement with the experimental data. This implies that the heat transfer rate on the wall is much more sensitive to the near wall model than the pressure coefficient.

Velocity and temperature profiles are shown in Fig. 3. The overall results agree very well with experimental data [21] except for the far downstream recovery region in which the numerical predictions do not recover so quickly to the ordinary boundary layer flow as in the experiment.

Forward facing step (strong streamwise acceleration)

Flows in a converging nozzle and over a turbine blade are examples of accelerating flow. Flow over a forward facing step is an example of a strong acce-

Table 3. Reattachment lengths for the backward facing step at $Re(H) = 28\,000$

	Exp. [21]	LS	NH	LB	Pr	Curvature [22]
X_R/H	6.66	5.5	5.9	5.5	6.3	5.9

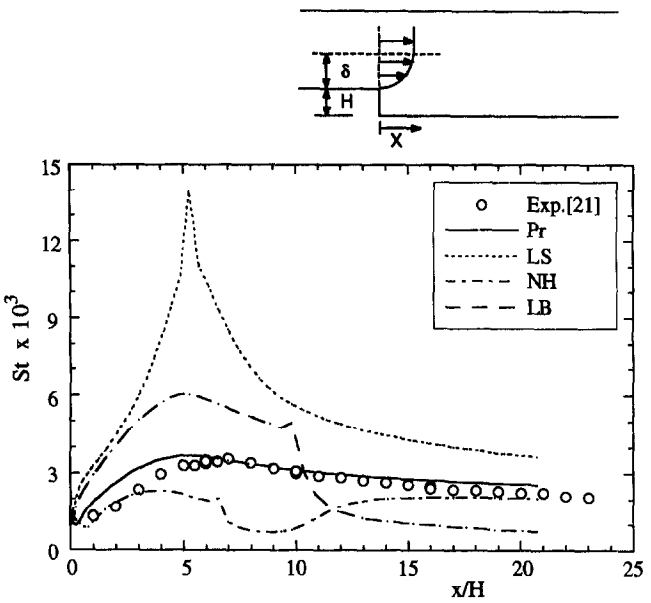

FIG. 2. Stanton number profiles for backward facing step flow at $Re(H) = 28\,000$ and $\delta/H = 1.1$.

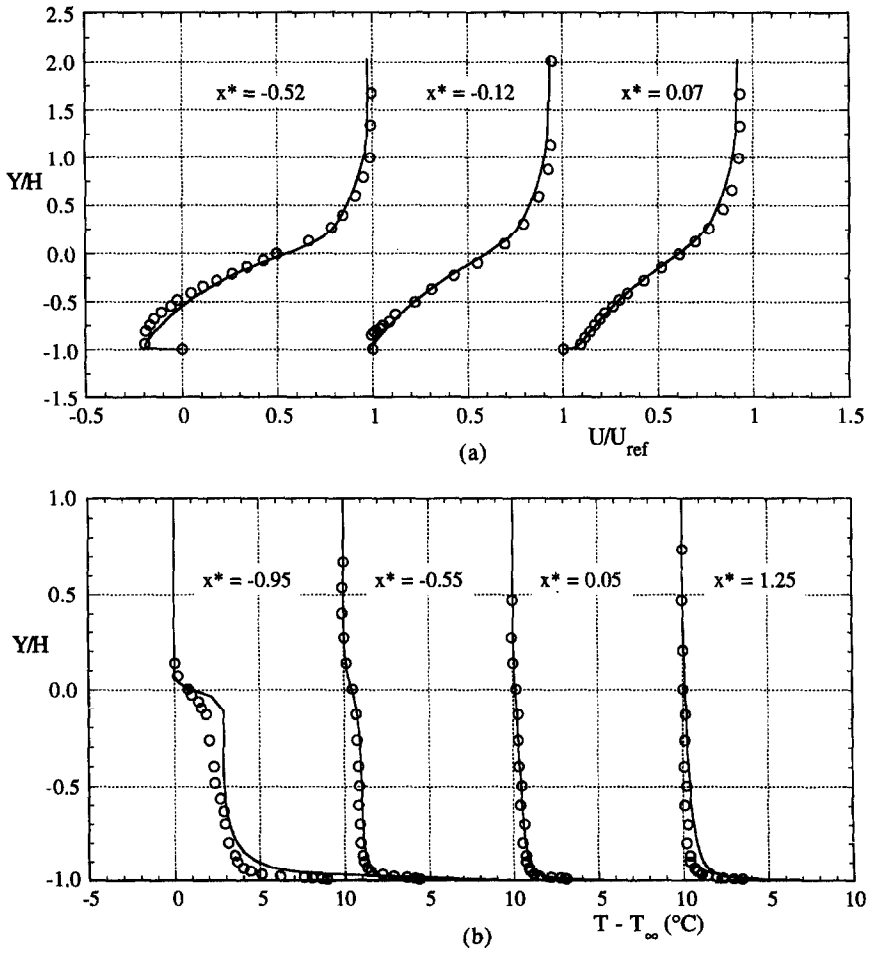

FIG. 3. Backward facing step flow at $Re(H) = 28\,000$ and $\delta/H = 1.1$. Comparison of present model with experiments of Vogel and Eaton [21]. (a) Mean velocity profiles. (b) Temperature profiles.

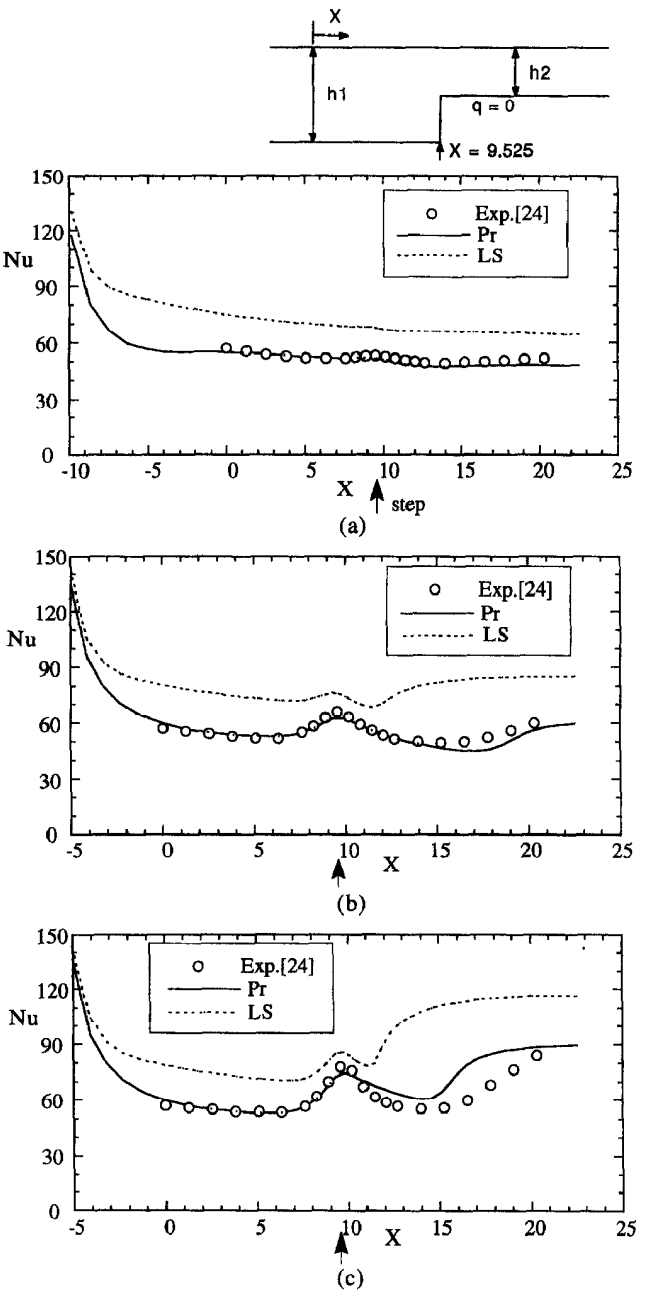

Fig. 4. $Nu(D_h)$ distributions on the top wall for forward facing step flow at $Re(D_h) = 18\,000$ with various step heights. (a) $h_2/h_1 = 0.936$. (b) $h_2/h_1 = 0.667$. (c) $h_2/h_1 = 0.496$.

lerating channel flow due to a sudden reduction of the cross sectional area. The initial turbulence is expected to dampen and the flow may even laminarize under the influence of strong acceleration. Originally, Jones and Launder [2] developed the low Reynolds number κ–ε model for laminarization of sink flow in which a turbulent flow becomes laminar. The calculated heat transfer rates and skin friction coefficients are compared with experimental data (Stanewich and Metzger [24]) and results from the LS model [23] in Figs. 4 and 5, respectively. *Nu* decreases continuously, reaching a fully-developed value, then increases just before the step at the start of the acceleration and thinned boundary layer. *Nu* decreases rapidly after the step when the viscous sublayer is thickened and the flow is laminarized due to a strong favorable pressure gradient. Finally, the flow recovers to the ordinary turbulent channel flow.

The peak Nusselt numbers on the upper surface near the position of the step increases with the step

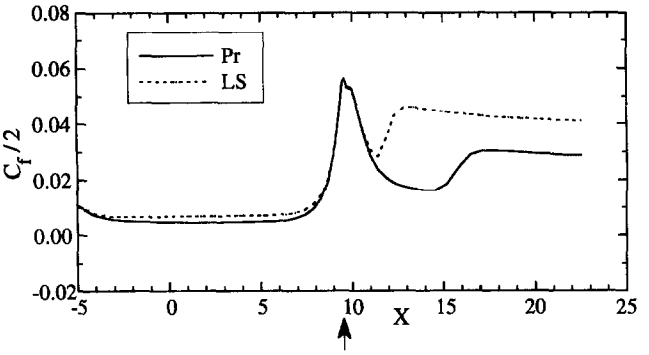

FIG. 5. Skin friction coefficients for forward facing step flow at $Re(D_h) = 18\,000$ and $h_2/h_1 = 0.496$.

height because the flow accelerates more (acceleration parameters,

$$K = \nu \frac{dU_m}{dx} \frac{1}{U_m^2}$$

which is determined by average velocity variation around the step, are 3.4, 21, and 71×10^{-6}, respectively). The present model predicts well the strong accelerating flow with laminarization. The LS model shows that the flow goes laminar then quickly return to turbulence. Jones and Launder's [3] numerical results also show that the turbulent flow starts earlier than found in the experiments for pipe and channel flows. The Nusselt numbers have a wide variation among the models despite the similar skin friction coefficients.

As examined in several flows, the present model accurately predicts the flow patterns and heat transfer rates. Increasing the Reynolds number, at high velocity flow, causes the numerical model values to show some discrepancy with experimental data. In general, the low-Reynolds-number κ–ε model is not suitable for high Reynolds number flow because there should be several grid points inside the viscous sublayer, which is numerically difficult at high Reynolds number flow due to the thin viscous sublayer.

NUMERICAL CALCULATION FOR ASYMMETRIC FLOWS

The two-dimensional flow through an array of normal flat plates is a fundamental problem for fluid flow and heat transfer. This kind of geometry is found in many systems, such as heat exchangers, a cascade of columns, and an array of slit jets. Recently, Milos *et al.* [25] calculated the velocity field for steady flow past a sudden cascade expansion (only downstream flow of the cascade) for laminar flow up to a Reynolds number of $Re(S) = 1000$. This showed the wake region length increases linearly with Reynolds number. The steady two-dimensional flow through a uniform cascade of flat plates was studied numerically by Ingham *et al.* [26]. Both papers dealt with low Reynolds number and assumed laminar flows. They also took the calculation domain between two geometrically symmetric lines as small as possible to reduce the calculation domain. This meant they always could get symmetric solutions.

Asymmetric streamlines for the flow past an array of circular cylinders were calculated by Singh *et al.* [27] with the distorted centerline of the cylinders. Ciofalo and Collins [19] got an asymmetric flow for a symmetric sudden expansion duct with the perturbed inlet boundary velocity profile, which was a small sinusoidal antisymmetric disturbance. The flow past a row of flat plates is similar to flow in a symmetric sudden expansion duct. The asymmetric flow in a symmetric sudden expansion duct is a well-known phenomenon. Similarly, the flow behind a row of cylinders has asymmetric wakes and streamlines. Flow visualization shows the asymmetric flow pattern for the flow around an array of rectangular cylinders (Cho *et al.* [28]).

The Navier–Stokes equations are nonlinear, so multiple solutions are possible. Also, asymmetric flow is possible in spite of the symmetric geometry and boundary conditions. A solution is shown in Fig. 6 for wake sizes behind an array of the rectangular cylinders. The stable asymmetric solutions exist only at high Reynolds numbers. One wake is much shorter than the other one. Both wake sizes are possible behind a cylinder, so there are two stable asymmetric solutions and one unstable symmetric solution. It is possible to get the asymmetric solutions in three ways. The first requires a slightly disturbed geometry (cf Singh *et al.* [27]) since no experimental geometry is perfect. In the second, a perturbed inlet boundary velocity profile is considered, as shown in Ciofalo's [19] calculation. These two methods are not designed for exactly symmetric geometry and boundary conditions. Finally, the initial velocity condition of the domain can be perturbed while keeping the symmetric geometry and boundary conditions. This condition exists naturally for example when a wind tunnel starts. For a given problem, the three approaches obtain essentially the same solutions for velocity profiles and local Sh/Nu on the cylinder surfaces.

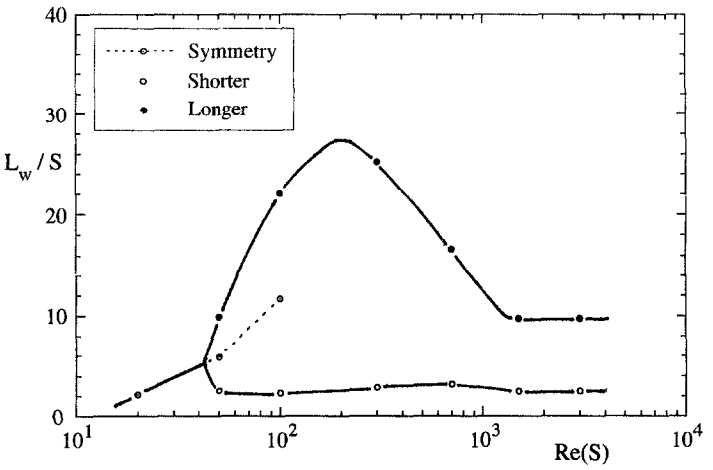

FIG. 6. Sizes of wake behind a row of rectangular cylinders (in streamwise direction).

Two-dimensional symmetric sudden expansion duct flow

Durst *et al.* [29] found a symmetric velocity profile for a Reynolds number of $Re(W_0) = 56$ and an asymmetric velocity profile for a Reynolds number greater than 114. The velocity distributions at the Reynolds number of 114 matched very well with the present model. The numerical solution predicts another separation bubble after the reattachment of the main stream on the side wall with a smaller wake at a Reynolds number of 250 (Fig. 7). The measured velocity profile did not show a bubble, but, as they mentioned, the shifted center of mainstream velocity and the flow visualization looks similar to the numerical results with respect to the separation bubble (Fig. 7).

Another comparison is made with Filetti and Kays' [30] measurements at a higher Reynolds number and with turbulent flow. The calculation domain uses the whole flow domain, not half of the domain even though it is a symmetric geometry about the centerline of the channel. The Nusselt number distributions on both long and short wake surfaces agree with experimental data (Fig. 8). The reattachment points of the present numerical model are almost the same as the experimental values. The profiles in Fig. 8 show differences in part because the maximum Nusselt numbers occur just before the reattachment points in the numerical calculation while Filetti and Kays [30] found the maximum heat transfer just after the reattachment. Some differences in the Nu inside the recirculation zone are attributable to the three-dimensional flow just after the step in the experiment. The numerical model predicts a small counter-rotating zone inside the recirculation zone for the assumed two-dimensional flow.

Flow through an array of two-dimensional rectangular cylinders

In the considered array of rectangular cylinders, the width of the rectangular cylinder is twice the slit width (spacing between the cylinders) and the thickness of the cylinder is chosen as 1.43 times the width of the slit (same as the experimental condition in Cho *et al.* [28]). The calculation domain is selected from the centerline of one cylinder to the centerline of the neighboring cylinder so that it includes one complete slit between them. As mentioned before, the half domain, which is the smallest possible geometrically symmetric domain, gives incorrect results (always symmetric solutions). To verify the selected domain, a double size control volume, including two complete slits, was tested and yielded the same results as the previous one. Three different perturbations, a small difference in size of the cylinders, a disturbed inlet flow boundary condition, and a sinusoidal perturbed initial velocity condition of the downstream part of the cylinders, were used and all yielded almost the same results for a test problem. After this, the last perturbation method was used.

A stable symmetric flow exists for a low Reynolds number of about 20. The symmetric solutions can be obtained numerically at Reynolds numbers of 50 and

FIG. 7. Streamlines for two-dimensional symmetric sudden expansion duct flow at $Re(H) = 250$ and $W/W_0 = 3$ (numerical).

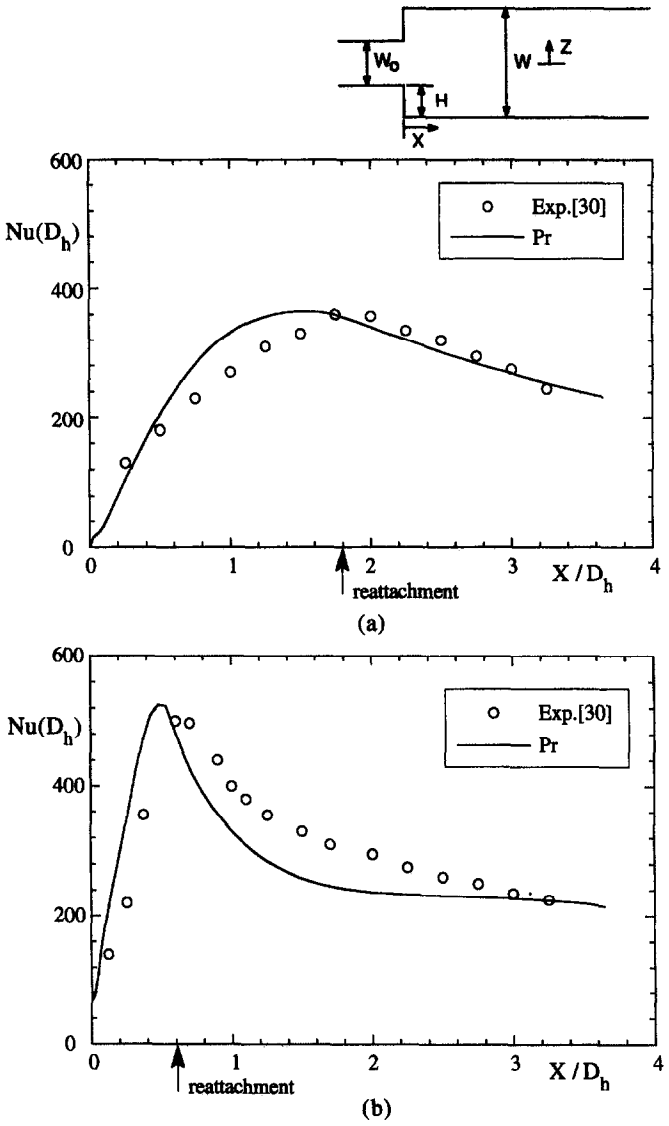

FIG. 8. $Nu(D_h)$ distributions for two-dimensional symmetric sudden expansion duct flow at $Re(D_h)$ = 70 000 and $W/W_o = 2.125$. Comparison of present model with experiments [30]. (a) Long recirculation side. (b) Short recirculation side.

100, but these go to asymmetric patterns and remain stable with a small perturbation. The length of wakes in the symmetric flow is between the lengths of shorter and longer wakes in the asymmetric flow (Fig. 6). A bifurcation point would be between the Reynolds numbers of 20 and 50. The symmetric solution did not exist numerically for the higher Reynolds numbers; it diverged and oscillated. The steady asymmetric solutions only exist to $Re_s = 300$ with one short wake and one long wake. With increasing Reynolds numbers, the flow becomes turbulent with the asymmetric pattern.

The wake sizes increase with Reynolds number in symmetric flow patterns such as the wake size following a single step in the laminar regime. In asymmetric flows, the sizes of the short wake change slightly with Reynolds number, but the long wakes increase continuously in the laminar flow regime until Reynolds numbers of 300. Then the long wake size decreases, and finally remains the same size at the Reynolds numbers of 1500 and 3000 in turbulence regime (Fig. 6), much like that for single step flows. From smoke wire visualization (Cho *et al.* [28]), the wake sizes are similar at Reynolds numbers of 1500 and 3000. The stream and/or streak line patterns match very well in both numerical and experimental results as shown in Fig. 9(a) and figures in ref. [28], respectively. The constant temperature contours (or constant density lines) show that most of the temperature changes occur in the near wall region (Fig. 9(b)).

Different grids, 78×44, 115×70, and 140×90, are used to verify the grid independence of the solution at Reynolds number of 1500. The Sherwood numbers

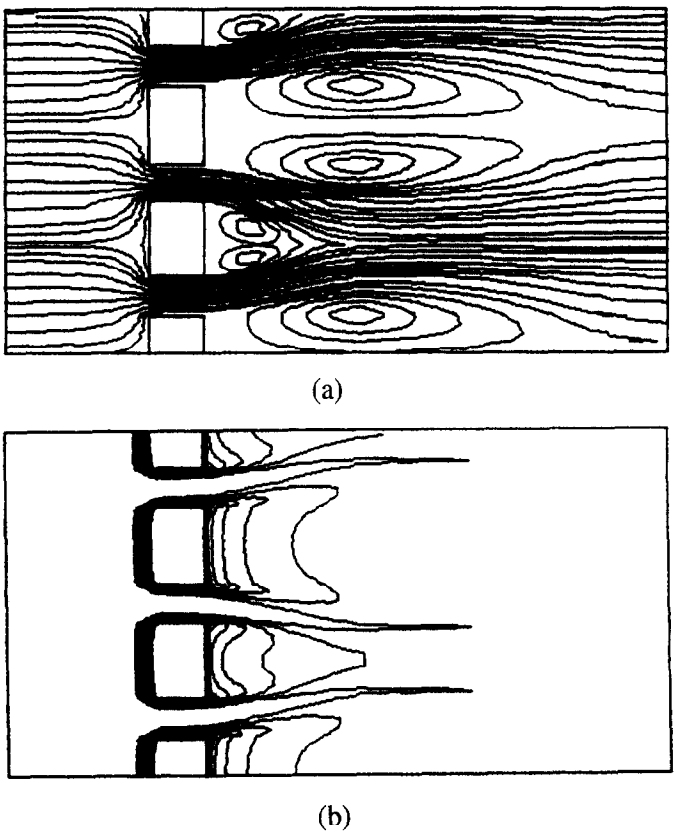

FIG. 9. Flow around an array of rectangular cylinders at $Re(S) = 1500$. (a) Streamlines. (b) Constant temperature contours.

on the upstream-facing surfaces are identical on the neighboring cylinders as expected for symmetric flow (Fig. 10), and these values do not change with the grid density. The Sherwood numbers on this surface compare well with the experimental results. The Sherwood numbers increase from the center to the sides due to acceleration of the flow and thinning of the boundary layer.

The Sherwood numbers on the inside surfaces changed and converged to the experimental result with increasing grid density. If the asymptotic method suggested by Churchill *et al.* [31] is applied, the present results would be even closer to the experimental data. The different sizes of the separation bubble and reattachment give different Sherwood numbers between two cylinders (Fig. 10). The largest discrepancy comes from the inside surface of the shorter wake cylinder due to the earlier reattachment point predicted numerically than found experimentally. There is a good prediction on the inside surface of the longer wake cylinder in which the flow does not reattach on the inside wall. The flow is laminar in most of the region and becomes turbulent at the end of the inside slit based on turbulent viscosity compared with laminar viscosity.

The Sherwood numbers on the leeward surfaces change a little from grid number 115×70 to 140×90. The peaks at the centerlines are due to the impingement effect of the recirculation in the wakes. The Sherwood number on the surfaces match fairly well with experimental data (Fig. 10) except at the end corner for both values of Re, which would be affected by the different upstream flow conditions (the different reattachment point inside slit, numerical/experimental).

CONCLUSION

A low-Reynolds-number κ–ε turbulence model has been developed to improve local heat transfer prediction in separated flows. The present paper also considers the asymmetric flow pattern due to instability in symmetric geometries, including a two-dimensional sudden expansion duct and an array of the rectangular cylinders. The model successfully predicts fluid flows and heat or mass transfer rates on the surfaces in several flow problems over a large Reynolds number range. However, the numerical prediction shows some variation from the experimental results at high Reynolds number. This could be due to the coefficient of f_μ which connects the fully turbulent flow to the wall where a molecular viscosity influences the turbulent structure. Another reason

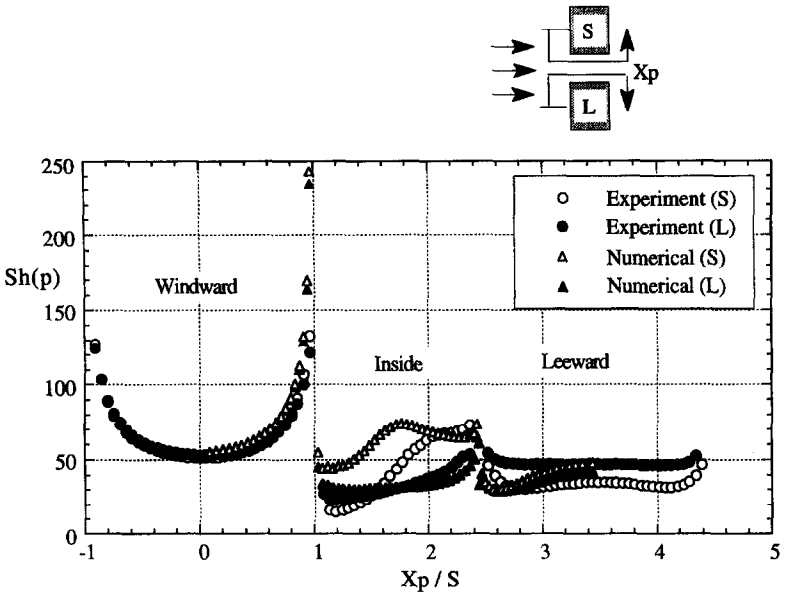

FIG. 10. $Sh(p)$ distributions for an array of rectangular cylinders at $Re(S) = 1500$: comparison of present model with experiments of Cho *et al.* [28]

might be the assumption for the turbulent Prandtl number near the wall which depends on local Reynolds number; sometimes the turbulent Prandtl number may be bigger than unity. These will be examined in a future study.

Acknowledgements—Support for this research came from the Air Force Office of Scientific Research, the Engineering Research Program of the Department of Energy, and the Minnesota Supercomputer Institute.

REFERENCES

1. C. C. Chieng and B. E. Launder, On the calculation of turbulent heat transport downstream from an abrupt pipe expansion, *Numer. Heat Transfer* **3,** 189–207 (1980).
2. W. P. Jones and B. E. Launder, The prediction of laminarization with a two-equation model of turbulence, *Int. J. Heat Mass Transfer* **15,** 301–314 (1972).
3. W. P. Jones and B. E. Launder, The calculation of low-Reynolds-number phenomena with a two-equation model of turbulence, *Int. J. Heat Mass Transfer* **16,** 1119–1130 (1973).
4. W. C. Reynolds, Computation of turbulent flows, *Ann. Rev. Fluid Mech.* **8,** 183–208 (1976).
5. C. K. G. Lam and K. A. Bremhorst, Modified form of the κ–ε model for predicting wall turbulence, *J. Fluids Engng* **103,** 456–460 (1981).
6. K. Hanjalic and B. E. Launder, Contribution towards a Reynolds-stress closure for low-Reynolds-number turbulence, *J. Fluid Mech.* **74,** 593–610 (1976).
7. C. Yap, Turbulent heat and momentum transfer in recirculating and impinging flows, Ph.D. Thesis, University of Manchester, U.K. (1987).
8. V. C. Patel, W. Rodi and G. Scheuerer, Turbulence models for near-wall and low Reynolds number flows: a review, *AIAA J.* **23,** 1308–1319 (1985).
9. X. F. Xu and K. T. Yang, Prediction of low Reynolds number turbulent wall jets and plumes with and without buoyancy, *Proceedings of the Ninth Int. Heat Transfer Conf.*, pp. 155–160. Hemisphere, Washington, DC (1990).
10. Y. Nagano and M. Hishida, Improved form of the κ–ε model for wall turbulent shear flows, *J. Fluids Engng* **109,** 156–160 (1987).
11. K.-Y. Chien, Predictions of channel and boundary-layer flows with a low-Reynolds-number turbulence model, *AIAA J.* **20,** 33–38 (1982).
12. S. V. Patankar, *Numerical Heat Transfer and Fluid Flow*. Hemisphere, McGraw-Hill, Washington, DC (1980).
13. P. S. Klebanoff, Characteristics of turbulence in a boundary layer with zero pressure gradient, NACA TN-3178 (1954).
14. J. Laufer, Investigation of turbulent flow in a two-dimensional channel, NACA Report 1053 (1951).
15. H. Eckelmann, The structure of the viscous sublayer and the adjacent wall region in a turbulent channel flow, *J. Fluid Mech.* **65,** 439–549 (1974).
16. B. E. Launder, On the computation of convective heat transfer in complex turbulent flows, *J. Heat Transfer* **110,** 1112–1128 (1988).
17. A. M. Gooray, C. B. Watkins and W. Aung, A two-pass procedure for the calculation heat transfer in recirculating turbulent flow, *Numer. Heat Transfer* **6,** 423–440 (1983).
18. R. S. Amano, Development of a turbulence near-wall model and its application to separated and reattached flows, *Numer. Heat Transfer* **7,** 59–75 (1984).
19. M. Ciofalo and M. W. Collins, κ–ε predictions of heat transfer in turbulent recirculating flows using an improved wall treatment, *Numer. Heat Transfer* **15,** 21–47 (1989).
20. M. Prud'homme and S. Elghobashi, Turbulent heat transfer near the reattachment of flow downstream of a sudden pipe expansion, *Numer. Heat Transfer* **10,** 349–368 (1986).
21. J. C. Vogel and J. K. Eaton, Heat transfer and fluid mechanics measurements in the turbulent reattaching flow behind a backward-facing step, Report MD-44, Thermo. Div., Dept. of M. E., Stanford Univ., California (1984).
22. M. A. Leschziner and W. Rodi, Calculation of annular

and twin parallel jets using various discretization schemes and turbulence-model variations, *J. Fluids Engng* **103,** 352–360 (1981).
23. B. E. Launder and B. I. Sharma, Application of the energy-dissipation model of turbulence to the calculation of flow near a spinning disc, *Lett. Heat Mass Transfer* **1,** 131–138 (1974).
24. B. J. Stanewich and D. E. Metzger, Local convection heat transfer on a plane wall in the vicinity of strong streamwise accelerations, *Heat Transfer in Gas Turbine Engines*, ASME-HTD Vol. **120,** pp. 65–70 (1989).
25. F. S. Milos, A. Acrivos and J. Kim, Steady flow past sudden expansions at large Reynolds number II. Navier–Stokes solutions for the cascade expansion, *Phys. Fluids* **30,** 7–18 (1987).
26. D. B. Ingham, T. Tang and B. R. Morton, Steady two-dimensional flow through a row of normal flat plates, *J. Fluid Mech.* **210,** 281–302 (1990).
27. P. Singh, P. H. Caussignac, A. Fortes, D. D. Joseph and T. Lungren, Stability of periodic arrays of cylinders across the stream by direct simulation, *J. Fluid Mech.* **205,** 553–571 (1989).
28. H. H. Cho, M. Y. Jabbari and R. J. Goldstein, Mass transfer with asymmetric flow through an array of rectangular cylinders, to appear in *J. Heat Transfer* (1994).
29. F. Durst, A. Melling and J. H. Whitelaw, Low Reynolds number flow over a plane symmetric sudden expansion, *J. Fluid Mech.* **64,** 111–128 (1974).
30. E. G. Filetti and W. M. Kays, Heat transfer in separated, reattached, and redevelopment regions behind a double step at entrance to a flat duct, *J. Heat Transfer* **89,** 163–168 (1967).
31. S. W. Churchill, P. Chao and H. Ozoe, Extrapolation of finite-difference calculations of laminar natural convection in enclosures to zero grid size, *Numer. Heat Transfer* **4,** 39–51 (1981).